JOURNAL OF GUIDANCE, CONTROL, AND DYNAMICS
Vol. 18, No. 6, November–December 1995

Comparative Stability Analysis and Performance of Magnetic Controllers for Bias Momentum Satellites

Hari B. Hablani*
Rockwell International Corporation, Downey, California 90241-7009

This paper reexamines magnetic controllers for roll/yaw control of Earth-pointing bias momentum satellites in circular orbits using pitch dipoles. A general magnetic controller employs three gains, first for controlling precession, second for damping nutations, and third for stiffening the roll/yaw motion directly, using attitude angles and rates for feedback. For an orbit-averaged magnetic field, dependence on these gains of the closed-loop roots associated with precession and nutation and their damping coefficients is investigated via eigenanalysis and root loci. Stability inequalities constraining the three gains are developed by applying Routh–Hurwitz criteria, and the stability boundaries so obtained are spot checked with Floquet theory. The stability and performance of a three-gain controller is compared with that of 1) the classical $\Delta h \times B$ controller and 2) controllers having zero stiffness gain with or without yaw feedback for precession. Faster transient performance and improved pointing accuracy attributed to yaw feedback and stiffness gain are clearly brought forth in this study. Simple formulas are developed to calculate the gains for desired precession rate and nutation damping coefficient.

I. Introduction

THIS paper is concerned with the design of linear magnetic attitude controllers for Earth-pointing bias momentum satellites in circular orbits. Certainly, since the successful demonstration of a magnetic controller for the television infrared observation satellite (TIROS)[1] in the early 1960s, these controllers have risen to a high degree of autonomy and sophistication; see, for example, the two controllers of the recent times for applications explorer mission[2] and relay mirror experiment[3] satellites. Nevertheless, gaps exist in the design techniques of magnetic controllers that have spurred the stability investigation reported here. Because of half-orbit periodic variation in the geomagnetic field for inclined orbits, techniques, such as Krylov–Bogoliubov averaging along with Lyapunov theory[4,5] and multiple time scales method,[6] have been used to determine suitable gains for desired stability and performance of the controllers. Wheeler[4,5] designed a two-gain control law for precession and nutation damping of axisymmetric spinning satellites, using feedback of transverse body rates and attitudes. Subsequently, Sorensen[7] designed a minimum-energy three-gain controller not only for precession and nutation damping but for stiffening the roll/yaw motion as well, analogous to the position feedback for single-axis controllers for zero-momentum satellites. Years later, Lebsock and Eterno[3] utilized this scheme to precess a bias momentum vector. In both of the works,[3,7] a Kalman filter is used to estimate roll/yaw attitudes and rates using roll measurements from horizon sensors and, in Ref. 3, yaw measurements from magnetometers. In contrast, Refs. 2, 6, and 8 designed magnetic controllers to damp nutations using the rate of change of the pitch magnetic field and to precess the angular momentum vector using only roll measurements from the horizon sensor without estimating yaw. Wheeler[4,5] and Alfriend[6] have developed stability inequalities between the precession and nutation gains, enabling one to select the gains for satisfactory nutation damping and precession. But no such stability analysis appears to exist for magnetic controllers that stiffen the roll/yaw motion as well. We are surprised to find that the advanced techniques mentioned have been applied for stability analysis, but more commonplace tools such as root locus and Routh–Hurwitz stability criteria have not been. The work of Rajaram and Goel[9] is an exception, but they only deal with near-equatorial orbits for which the geomagnetic field is essentially constant, and use, effectively, only roll and roll rate for control and a roll dipole. Granted that half-orbit periodic variation in the magnetic field of inclined orbits, leading to periodic coefficients in the governing linear attitude equations of motion, may have deterred such attempts, but surely the accuracy of the analytical results based on averaged coefficients can be checked via Floquet theory and time-domain simulation.

This brings us to the contents of this paper. Section II deals with the classical one-gain $\Delta \boldsymbol{h} \times \boldsymbol{B}$ momentum removal policy[10] for modulating the pitch dipole moment to effect the roll/yaw control; here, $\Delta \boldsymbol{h}$ is the excess, unwanted angular momentum of an Earth-pointing bias momentum satellite and $\boldsymbol{B}$ the geomagnetic field. Because of the presence of only one gain, this policy leads to a constraint between precession and nutation gains that is, unexpectedly, one of the stability boundaries formulated by Wheeler[4,5] and Alfriend.[6] The three-gain pitch dipole modulation policy is studied in Sec. III, wherein three additional constants associated with yaw feedback are introduced so that various control policies of the past can be recreated by assigning special values to the gains. Roll/yaw magnetic control torques are averaged, and the stability inequality relating the precession, nutation, and stiffness gains is developed by applying Routh–Hurwitz stability criteria. Since the nutation frequency is typically much higher than the orbit frequency, the satellite's moments of inertia and nutation gains are zeroed for preliminary selection of the precession and stiffness gains, and the two first-order equations of bias momentum precession are investigated in the first part of Sec. IV, where the relationships of precession time constants with the control gains are also developed. In the second part, the nutation gain is related to the nutation damping coefficient or associated time constant by an eigenanalysis of the equations of motion governing inertial roll/yaw rates of the spacecraft. This analysis is based on the assumption that since the nutation damping takes place much faster than the precession, the precession and stiffness gains can be ignored and the geomagnetic field can be treated as invariant over a short orbital arc during which the nutation damping takes place. In Sec. V, the closed-loop precession and nutation roots and the corresponding damping coefficients are determined numerically for a large range of precession and nutation gains; these roots are then compared with analytic roots and discussed in depth for each of the controllers. Stability boundaries based on the average magnetic field are compared with discrete Floquet stability results and with those using other advanced techniques.[4,6] Section VI, finally, concludes the paper.

Received Oct. 9, 1993; revision received June 12, 1995; accepted for publication July 17, 1995.

*Senior Engineering Specialist, Advanced Programs, Avionics and Software Group, Space Systems Division, 12214 Lakewood Boulevard. Associate Fellow AIAA.

II. $\Delta h \times B$ Control Policy for Angular Momentum Precession

Consider a bias momentum Earth-pointing satellite in a circular orbit, with its nominal wheel momentum vector $\boldsymbol{h}_s = h_s \boldsymbol{c}_2$ along

the orbit normal; here, $\boldsymbol{c}_2$ is a unit vector aligned with the nominal orientation of the pitch axis opposite to the orbit normal and defined such that the nominal once-per-orbit clockwise rotation rate of the satellite for Earth pointing is given by $-\omega_0 \boldsymbol{c}_2 (\omega_0 > 0)$. Accordingly, although not mandatory, the constant wheel momentum h_s is also clockwise and so less than zero. Let α_1, α_2, and α_3 be the infinitesimal roll, pitch, and yaw angles of the spacecraft, respectively, and $\dot{\alpha}_1$, $\dot{\alpha}_2$, and $\dot{\alpha}_3$ be their rates. It can then be shown, under the assumption that

$$|h_s| \gg \{\max(I_1, I_2, I_3)\}\omega_0 \tag{1}$$

that the extraneous angular momentum $\Delta \boldsymbol{h}$ in the local-vertical-local-horizontal orbit frame $\mathcal{F}^c$, not spacecraft body frame $\mathcal{F}^b$, is approximately given by

$$\Delta \boldsymbol{h}^{\mathcal{F}^c} = \{I_1 \dot{\alpha}_1 - h_s \alpha_3 \quad 0 \quad I_3 \dot{\alpha}_3 + h_s \alpha_1\}^T \triangleq [h_1 \quad 0 \quad h_3]^T \tag{2}$$

where x and z components are along the local velocity vector and nadir, respectively; these two directions also define the unit vectors $\boldsymbol{c}_1$ and $\boldsymbol{c}_3$, respectively, forming with $\boldsymbol{c}_2$ a right-handed frame $\mathcal{F}^c$. In Eq. (1), I_1, I_2, and I_3 are the spacecraft's central, principal moments of inertia in the body-fixed frame $\mathcal{F}^b$, and the superscript T denotes transpose. In the presence of a well-designed nutation damper, the terms $I_i \dot{\alpha}_i$ are usually negligible compared to the momentum $h_s \alpha_i$ $(i = 1, 3)$, but since one of the objectives of the magnetic controllers designed here is to damp the nutations, these terms will be retained in the analysis.

To control the roll/yaw angles according to the $\Delta \boldsymbol{h} \times \boldsymbol{B}$ law, the pitch dipole moment m_2 residing in the spacecraft must vary in proportion to[10]

$$m_2 \propto h_3 B_1 - h_1 B_3 \tag{3}$$

where h_1 and h_3 are defined by Eq. (2) and B_1 and B_3 are the components of $\boldsymbol{B}$ along the $\boldsymbol{c}_1$ and $\boldsymbol{c}_3$ unit vectors. The pitch electromagnet is fixed to the spacecraft body along the pitch axis, so it is not along $\boldsymbol{c}_2$ as implied by Eq. (3); but it is nearly so for small α_1 and α_3 angles and, therefore, Eq. (3) is valid within this linear range. Also, by using only a pitch dipole for the roll/yaw control, this analysis is rendered inapplicable for the satellites in the orbits near the equator where a pitch dipole is essentially parallel to the geomagnetic field and, therefore, not used to produce a roll/yaw control torque. Now, returning to Eq. (3), let K_α be the constant of proportionality. Substituting h_1 and h_3 from Eq. (2), we arrive at

$$m_2 = K_\alpha h_s (B_1 \alpha_1 + B_3 \alpha_3) - K_\alpha (B_3 I_1 \dot{\alpha}_1 - B_1 I_3 \dot{\alpha}_3) \tag{4}$$

To conform with the control policies extant in the literature, the policy of Eq. (4) is altered to

$$m_2 = K_\alpha h_s (B_1 \alpha_1 + B_3 \alpha_3) - K_\alpha \sqrt{I_1 I_3} (B_3 \dot{\alpha}_1 - B_1 \dot{\alpha}_3) \tag{5}$$

The first term in the right-hand side of Eq. (5) precesses the angular momentum vector from its drifted position $h_s(-\alpha_3 \boldsymbol{c}_1 + \boldsymbol{c}_2 + \alpha_1 \boldsymbol{c}_3)$ to $h_s \boldsymbol{c}_2$, whereas the second term damps the rates $\dot{\alpha}_1$ and $\dot{\alpha}_3$, nutation damping. Accordingly, the gains K_α and $K_\alpha \sqrt{(I_1 I_3)}$ in Eq. (5) could be denoted, more appropriately, as k_p and k_n, transforming Eq. (5) to

$$m_2 = k_p h_s (B_1 \alpha_1 + B_3 \alpha_3) - k_n (B_3 \dot{\alpha}_1 - B_1 \dot{\alpha}_3) \tag{6}$$

where, by definition, k_n and k_p are constrained by the relationship

$$k_n = k_p \sqrt{I_1 I_3} \tag{7}$$

Finally, the roll and yaw control torques, g_{c1} and g_{c3}, respectively, produced by the pitch dipole are

$$g_{c1} = m_2 B_3, \qquad g_{c3} = -m_2 B_1 \tag{8}$$

For the purpose of stability analysis, the tilted dipole model of the geomagnetic field $\boldsymbol{B}$ is used here. Expressing the field in the rotating orbit frame $\mathcal{F}^c$, one has[10]

$$\boldsymbol{B}^{\mathcal{F}^c} = \hat{\mu}_m [s\xi_m c(\omega_0 t - \eta_m), \quad -c\xi_m, \quad 2s\xi_m s(\omega_0 t - \eta_m)]^T \tag{9}$$

where $s()$ and $c()$ are sin() and cos(), $\hat{\mu}_m = \mu_m / r^3$,

$$c\xi_m = ci\, c\gamma_m + si\, s\gamma_m\, c\beta'_m \tag{10a}$$

$$s\eta_m s\xi_m = -s\gamma_m s\beta'_m \tag{10b}$$

$$c\eta_m s\xi_m = si\, c\gamma_m - ci\, s\gamma_m\, c\beta'_m \tag{10c}$$

$$\beta'_m = \beta_m + \omega_e t - \Omega_{an} \tag{10d}$$

and the tilt angle $\gamma_m = 11.44$ deg. Furthermore, μ_m is the Earth's dipole strength ($7.943e15$ Weber · m), r the spacecraft's orbit radius, and $\omega_0 t$ the spacecraft's true anomaly measured from the ascending node line. The pitch and nadir components of $\boldsymbol{B}^{\mathcal{F}^c}$ in Eq. (9) are negative of the orbit normal and zenith components, respectively, in Eq. (A.12) of Ref. 10. Equations (10a) and (10b), defining the angles ξ_m and η_m, are identical to Eqs. (A.14) and (A.15) of Ref. 10; the supplementary Eq. (10c), consistent with Eqs. (10a) and (10b) and not presented in Ref. 10, is necessary to arrive at Eq. (9). Physically, the angle ξ_m is the instantaneous inclination of the spacecraft orbit with the geomagnetic equator, and η_m is the angle from the ascending node of the orbit relative to the Earth's equator to the ascending node relative to the geomagnetic equator. The slow variation of the angles ξ_m and η_m, compared with the fast variation of the orbit angle $\omega_0 t$, arises from the Earth's rotation $\omega_e t$ and the nodal regression; Ω_{an} in Eq. (10d) is the instantaneous ascending node angle of the spacecraft orbit. The angle $\beta_m + \omega_e t$ in Eq. (10d) is the angle between the vernal equinox and the instantaneous line of intersection of the equatorial plane with the geomagnetic equator (β_m being its initial value). And, finally, the angle i is the orbit inclination. For further details on the geomagnetic field, see Refs. 10 and 11.

The field components B_1 and B_3 in Eqs. (8) are in the spacecraft body frame $\mathcal{F}^b$, but for linear analysis $\boldsymbol{B}^{\mathcal{F}^b} \approx \boldsymbol{B}^{\mathcal{F}^c}$ and so the B_1 and B_3 components from Eq. (9) can be substituted in Eqs. (6) and (8). This leads to the torques g_{c1} and g_{c3} containing time-varying terms at twice the orbit rate. To apply Routh–Hurwitz stability criteria, the following average values of these torque expressions are then arrived at:

$$\begin{aligned} g_{c1,\mathrm{av}} &= -2k'_n \dot{\alpha}_1 + 2k'_p h_s \alpha_3 \\ g_{c3,\mathrm{av}} &= -\tfrac{1}{2} k'_n \dot{\alpha}_3 - \tfrac{1}{2} k'_p h_s \alpha_1 \end{aligned} \tag{11}$$

where the gains k'_n and k'_p are functions of the angle ξ_m:

$$k'_n \triangleq k_n \hat{\mu}_m^2 \sin^2 \xi_m, \qquad k'_p \triangleq k_p \hat{\mu}_m^2 \sin^2 \xi_m \tag{12}$$

Note that for untilted dipole model $\gamma_m = 0$, and then $\xi_m = i$ and $\eta_m = 0$.

Under the approximation (1), the roll/yaw equations of a triaxial bias momentum Earth-pointing satellite in a circular orbit are given by [see Hughes,[12] Eqs. (6)]

$$\begin{aligned} I_1 \ddot{\alpha}_1 - h_s \dot{\alpha}_3 - h_s \omega_0 \alpha_1 &= g_{c1} \\ I_3 \ddot{\alpha}_3 + h_s \dot{\alpha}_1 - h_s \omega_0 \alpha_3 &= g_{c3} \end{aligned} \tag{13}$$

For Routh–Hurwitz stability analysis, the average control torques (11) are substituted in Eqs. (13), and the following characteristic equation then ensues:

$$s^4 + a_1 s^3 + a_2 s^2 + a_3 s + a_4 = 0 \tag{14}$$

with s as the Laplace variable corresponding to the orbit angle $\omega_0 t$. The explicit expressions of the polynomial coefficients can be derived from the general a presented later [Eqs. (21)], but for now we note that, in view of the relationship (7) between k_n and k_p, the stability analysis leads to the condition $k_n > 0$ for $h_s < 0$, and to the following more predominant condition:

$$\Delta_3 = a_1 (a_2 a_3 - a_1 a_4) - a_3^2 > 0 \tag{15}$$

It turns out that this condition is violated if $I_1 = I_3$ and if the relationship (7) between the nutation and precession gains is satisfied, because then for $I_1 = I_3$ and $k_n = k_p I_1$

$$\Delta_3 = 0 \tag{16}$$

Hence we conclude that the $\Delta \boldsymbol{h} \times \boldsymbol{B}$ law is unstable for a bias momentum satellite with roll/yaw inertial symmetry. As this conclusion is based on the averaged magnetic field, it must be verified by Floquet theory; nonetheless, it is noteworthy that Eq. (7) indeed agrees with the stability boundaries for inertially symmetric satellites determined by Wheeler[4] using Lyapunov theory and Alfriend[6] [his Eq. (27), simplified using the approximation (1) here]. This instability is caused by insufficient nutation damping gain k_n. For asymmetric satellites ($I_1 \neq I_3$), we are unable to prove analytically, even under the approximation (1), that with the relationship (7) the inequality (15) reduces to an equality, but it is found so numerically, as illustrated in Sec. V.

The preceding stability results suggest that the nutation damping gain k_n should be made independent of k_p so that an appropriate lower limit on k_n may be developed to ensure stability; the upper limit will arise from noise in roll/yaw rate estimates, but that topic will not be addressed here. The controller may, indeed, be made even more versatile by adding a third gain—stiffness gain—to impart stiffness to the roll/yaw motion, as stated in the Introduction. One such general controller is considered next.

III. Magnetic Controller for Precession, Nutation Damping, and Stiffness

The modulation law, Eq. (6), for a pitch dipole moment, is generalized and augmented to incorporate the stiffness gain k_s as follows:

$$m_2 = k_p h_s (B_1 \alpha_1 + \chi_p B_3 \alpha_3) - k_n (B_3 \dot{\alpha}_1 - \chi_n B_1 \dot{\alpha}_3) - k_s (B_3 \alpha_1 - \chi_s B_1 \alpha_3) \tag{17}$$

The form of the last term—the stiffness term—resembles that of the nutation damping term because they are both intended to influence the roll and yaw angles and rates directly. Additionally, the parameters χ_p, χ_n, and χ_s are introduced so that by equating them to zero the yaw and yaw rate can be eliminated if not available for feedback, or they may be assigned special values to lay desired emphasis on yaw signals. To examine Routh–Hurwitz stability, roll/yaw control torques are obtained by substituting Eq. (17) and the time-varying magnetic field, Eq. (9), into Eq. (8). The terms varying at twice the orbit rate are then averaged and we arrive at

$$g_{c1,\mathrm{av}} = -2k_n' \dot{\alpha}_1 + 2k_p' h_s \chi_p \alpha_3 - 2k_s' \alpha_1 \tag{18a}$$

$$g_{c3,\mathrm{av}} = -\tfrac{1}{2} k_n' \chi_n \dot{\alpha}_3 - \tfrac{1}{2} k_p' h_s \alpha_1 - \tfrac{1}{2} k_s' \chi_s \alpha_3 \tag{18b}$$

where the gain k_s' is defined as, similar to the definitions (12),

$$k_s' \triangleq k_s \hat{\mu}_m^2 \sin^2 \xi_m \tag{19}$$

Equations (18) reveal that the gains k_n' and k_s' must be each positive, as the gains usually are, to achieve nutation damping and stiffen the roll/yaw motion. That the precession gain k_p should also be positive is not immediately clear, but it is found so from the stability analysis. The form of the control torques (18) is the same as those considered by Sorensen[7] and Lebsock and Eterno,[3] and the laws of Alfriend[2] and Wheeler[4] are special cases thereof, considered subsequently in some detail. The average torques (18) are now inserted in the simplified motion equations (13), and time t is replaced by the orbit angle $\omega_0 t$ for differentiation. The following nondimensional parameters then emerge:

$$\hat{k}_{n1} \triangleq k_n'/(I_1 \omega_0), \qquad \hat{k}_p \triangleq k_p'/\omega_0, \qquad \hat{k}_{s1} \triangleq k_s'/(I_1 \omega_0^2)$$
$$\hat{J}_{si} \triangleq h_s/(I_i \omega_0), \qquad i_a \triangleq I_1/I_3 \qquad (i = 1, 2, 3) \tag{20}$$

where $\hat{J}_{si}$ is a bias momentum parameter and i_a a roll/yaw inertial asymmetry parameter. Also recall that $h_s < 0$, so $\hat{J}_{si} < 0$. The fourth order characteristic polynomial, Eq. (14), has the following coefficients now:

$$a_1 \triangleq \hat{k}_{n1}\left(2 + \tfrac{1}{2} i_a \chi_n\right)$$
$$a_2 \triangleq 2\hat{k}_{s1} - \hat{J}_{s1} + i_a\left[\hat{k}_{n1}^2 \chi_n + \tfrac{1}{2}\hat{k}_{s1}\chi_s - \hat{J}_{s1} + \hat{J}_{s1}^2\right]$$
$$a_3 \triangleq i_a\left[\tfrac{1}{2}\hat{k}_{n1}\chi_n(-\hat{J}_{s1} + 2\hat{k}_{s1}) + 2\hat{k}_{n1}\left(-\hat{J}_{s1} + \tfrac{1}{2}\hat{k}_{s1}\chi_s\right) + \hat{J}_{s1}^2\hat{k}_p\left(\tfrac{1}{2} + 2\chi_p\right)\right] \tag{21}$$
$$a_4 \triangleq i_a\left[\left(-\hat{J}_{s1} + \tfrac{1}{2}\hat{k}_{s1}\chi_s\right)(-\hat{J}_{s1} + 2\hat{k}_{s1}) + \hat{J}_{s1}^2\hat{k}_p^2\chi_p\right]$$

The necessary condition for stability, that none of the a be negative, is easily satisfied by requiring that the three control gains be positive and the bias momentum h_s negative. (The circumstance $h_s > 0$, although possible, is not examined here.) A necessary and sufficient condition for stability is the condition (15), but with lengthy coefficients and several parameters involved, it is infeasible to develop a simple parametric inequality; special cases of the modulation policy (17), employed by prior investigators, are therefore considered.

$\Delta \boldsymbol{h} \times \boldsymbol{B}$ Policy

This is the policy (6) obtained from Eq. (17) for the specific values $k_s = 0$, $\chi_n = 1 = \chi_p$, and the nondimensional version of the relationship (7)

$$\hat{k}_{n1} = \hat{k}_p/\sqrt{i_a} \tag{22}$$

Because $|\hat{J}_{si}| \gg 1$ $(i = 1, 2, 3)$, one can prove Eq. (16) literally for equal or just slightly different roll and yaw principal moments of inertia. Subsequently in Sec. V, we will show through a numerical example that Δ_3 equals zero (and, hence, controller unstable—nutational instability) even for a substantial roll/yaw inertial asymmetry: $i_a = 1.36$.

Alfriend's Law

Stickler and Alfriend[8] analyzed the modulation policy

$$m_2 = -K_1 B_1 \alpha_1 - K_2 (B_3 \dot{\alpha}_1 - B_1 \dot{\alpha}_3) \tag{23}$$

where K_1 and K_2 (notations of Ref. 8) are precession and nutation gains related to k_p and k_n as established next. (Because of sign conventions, K_1 in Ref. 8 is $-K_1$ here.) The general policy (17) specializes to the policy (23) if $k_s = 0$, $\chi_n = 1$, and $\chi_p = 0$ for no yaw feedback. And then, comparing Eq. (23) with Eq. (17), the gains K_1 and K_2 are found to be

$$K_1 = -k_p h_s, \qquad K_2 = k_n \tag{24}$$

where K_1 is positive because h_s is negative, and k_p is positive.

The stability condition (27) of Ref. 8 associated with the policy (23) here and derived on the basis of energy principle is a function of the instantaneous location of the spacecraft in the orbit. It is most severe at the nodes, where it reduces to, by virtue of the relationship (24),

$$k_n > \sqrt{I_1 I_3}\, k_p \tag{25}$$

which yields the stability boundary (7) corresponding to the $\Delta \boldsymbol{h} \times \boldsymbol{B}$ law. Other stability conditions that involve a weak yaw feedback and are derived using the multiple time scale approach are the conditions (25) and (27) of Ref. 6. In view of the approximation (1) and the correspondence (24), these conditions reduce to

$$k_n > [I_1 I_3/(I_1 + 4I_3)]k_p \tag{26a}$$

$$k_n > I_3 k_p \tag{26b}$$

where Eq. (26a) is for the average nutational stability and Eq. (26b) is a stricter requirement for the same.

In Sec. V, we compare the stability condition (15) with Eqs. (25) and (26) and the discrete stability boundary determined by using Floquet theory.

Wheeler's Law

When the yaw angle can be measured or estimated, it is desirable to use it along with the roll measurement from horizon sensors, because the two angles together determine the orientation of the drifted angular momentum vector in the celestial sphere. Wheeler,[4] therefore, analyzed a pitch dipole modulation policy that uses yaw and yaw rate, in addition to roll and roll rate. This policy is obtained from the general policy (17) by substituting $k_s = 0$, $\chi_p = 1 = \chi_n$. The associated stability condition, Eq. (17) of Ref. 5, turns out to be the same as the condition (25) or (26b) (for $I_1 = I_3$) after resolving notational differences and recalling the approximation (1).

Lebsock–Eterno's Law

To reduce the number of independent parameters in Eq. (17) and to symmetrize the average roll/yaw control torques, Eqs. (18), we assign the following special values to the yaw feedback parameters and link the stiffness and precession gains:

$$h_s k'_p = -4k'_s, \qquad \chi_n = 4 = \chi_s, \qquad \chi_p = \tfrac{1}{4} \tag{27}$$

yielding thereby

$$g_{c1,\mathrm{av}} = -2k'_n\dot{\alpha}_1 + \tfrac{1}{2}h_s k'_p\alpha_3 + \tfrac{1}{2}h_s k'_p\alpha_1 \tag{28}$$

$$g_{c3,\mathrm{av}} = -2k'_n\dot{\alpha}_3 - \tfrac{1}{2}h_s k'_p\alpha_1 + \tfrac{1}{2}h_s k'_p\alpha_3 \tag{29}$$

Because of the stipulated relationship (27a) between k_p and k_s, we now have only k_p and k_n gains in Eqs. (28) and (29). This form is the same as the one used by Lebsock and Eterno[3] and so the control law at hand will be called Lebsock–Eterno's law. Perhaps surprisingly, if the relationship (27a) is not used, we will arrive at the torques $g_{c1,\mathrm{av}}$ and $g_{c3,\mathrm{av}}$ identical to Eq. (15) of Sorensen,[7] based on the minimum-energy linear optimal control theory, and the torques will then involve k_p, k_n, and k_s. To conduct a Routh–Hurwitz stability analysis, the a in Eqs. (21) are simplified using Eq. (27), and the stability condition Δ_3 is then written as a second-degree polynomial in $\hat{k}_p$ to delineate the stability boundary in the $\hat{k}_{n1}$–$\hat{k}_p$ plane. Corresponding numerical results are shown in Sec. V.

IV. Selection of Gains for Precession and Nutation Damping

Nutation amplitude as compared to the angular momentum drift is usually very small, and because of large frequency separation (nutation frequency may be 50–2000 times the precession frequency ω_0 in the rotating orbit frame), nutation may be damped much faster than the precession of a momentum vector. For example, if the nutation frequency Ω_n is 1.16 rad/s and the orbit frequency ω_0 is 0.7E-3 rad/s, then $\Omega_n/\omega_0 = 1660$; and with nutation damping coefficient $\zeta_n = 0.1$, a nutation amplitude will decrease to its 1% value in mere 1.6 deg of orbit travel, with little change in the geomagnetic field. (Nutation is persistently excited though by precession.) This suggests that for a preliminary determination of the gains, the precession and nutation dynamics could be treated separately (analogous to the approaches of Refs. 4, 8, 13, and 14) leading to simple relationships between gains and time constants or damping coefficients. Such relationships are developed in the following.

Precession Control

Nutation-free dynamics of a bias momentum Earth-pointing satellite in the orbit frame $\mathcal{F}^c$ is governed by

$$\dot{h}_1 - \omega_0 h_3 = g_{c1} \tag{30a}$$

$$\dot{h}_3 + \omega_0 h_1 = g_{c3} \tag{30b}$$

where the angular momentum components h_1 and h_3 along $\boldsymbol{c}_1$ and $\boldsymbol{c}_3$ unit vectors are defined by

$$h_1 \triangleq -h_s\alpha_3, \qquad h_3 \triangleq h_s\alpha_1 \tag{31}$$

which differ slightly from the definitions in Eq. (2). As is well known, Eqs. (30) and (31) can be obtained from Eqs. (13) and (2) by zeroing the spacecraft's moments of inertia. To determine average performance of a magnetic controller, the average torques $g_{c1,\mathrm{av}}$ and $g_{c3,\mathrm{av}}$ from Eqs. (18) are substituted in Eqs. (30) with $k'_n = 0$. We next define a nondimensional stiffness gain $\hat{k}_s$,

$$\hat{k}_s = -k'_s/(h_s\omega_0) = -\hat{k}_{s1}/\hat{J}_{s1} \tag{32}$$

where since $h_s < 0$, $\hat{k}_s > 0$. The complex pair of the nondimensional roots of Eqs. (30) is

$$s = -\left(\tfrac{1}{4} + \chi_p\right)\hat{k}_p \pm j\Big[\hat{k}_p^2\chi_p + \left(1 + \tfrac{1}{2}\hat{k}_s\chi_s\right)\left(1 + 2\hat{k}_s\right) - \left(\tfrac{1}{4} + \chi_p\right)^2\hat{k}_p^2\Big]^{\frac{1}{2}} \tag{33}$$

where $j^2 = -1$. As expected, if $\hat{k}_p$ and $\hat{k}_s$ are both zero (and $\hat{k}_n$ is zero already), the complex roots reduce to $s = \pm j1$ (the nondimensional orbit frequency of the Earth-pointing orbit frame). Also, the stiffness gain $\hat{k}_s$ does not contribute to the real part of the roots (33). Clearly, the time constant in terms of orbit angle for precessing a momentum vector is $[(\frac{1}{4} + \chi_p)\hat{k}_p]^{-1}$ rad. Three special cases of the roots (33) are considered now.

Roll/Yaw Feedback with $k_s = 0$ (Wheeler's and $\Delta\boldsymbol{h} \times \boldsymbol{B}$ Laws)

The roots (33) now reduce to

$$s = -\left(\tfrac{1}{4} + \chi_p\right)\hat{k}_p \pm j\Big[1 - \hat{k}_p^2\left(\tfrac{1}{4} - \chi_p\right)^2\Big]^{\frac{1}{2}} \triangleq -\zeta_p\omega_p \pm j\omega_p\sqrt{1 - \zeta_p^2} \tag{34}$$

with no change in the time constant calculated. The damping coefficient ζ_p and the undamped precession frequency ω_p are

$$\omega_p^2 \triangleq 1 + \hat{k}_p^2\chi_p, \qquad \zeta_p \triangleq \left(\tfrac{1}{4} + \chi_p\right)\hat{k}_p/\omega_p \tag{35}$$

For χ_p equal to unity, ω_p and ζ_p simplify to

$$\omega_p^2 \triangleq 1 + \hat{k}_p^2, \qquad \zeta_p \triangleq 5\hat{k}_p\Big/\Big[4\sqrt{1 + \hat{k}_p^2}\Big] \tag{36}$$

To preclude real roots, the requirement $\zeta_p < 1$ may be imposed, which then leads to the condition $\hat{k}_p < \frac{4}{3}$, with two equal real roots being $(-\frac{5}{3})$ when $\zeta_p = 1$ and $\hat{k}_p = \frac{4}{3}$. We also note that the results (34–36) will alter if the nutation gain k_n is reinserted in the eigenanalysis.

Alfriend's Law

This is a further specialization of the given case in that it does not use yaw feedback, implying $\chi_p = 0$ in the policy (17). The roots (34) and ω_p and ζ_p now reduce to

$$s \triangleq -\hat{k}_p/4 \pm j\sqrt{1 - \hat{k}_p^2/16}; \qquad \omega_p = 1, \qquad \zeta_p = \hat{k}_p/4 \tag{37}$$

which are, indeed, the same as those stated by Stickler and Alfriend.[8] For comparison, note that in addition to the equivalence (24) their K^* is the same as $\hat{k}_p$ here, and so the reason for their recommendation $1 < \hat{k}_p < 3$ is to keep $0.25 \le \zeta_p \le 0.75$.

Lebsock–Eterno's Law

Alfriend's law does not use yaw feedback so the corresponding closed-loop undamped frequency, Eq. (37), remains unity regardless of $\hat{k}_p$. Wheeler's law, in contrast, employs yaw feedback, so the corresponding ω_p and ζ_p, Eqs. (36) (k_n and k_s both zero), ascend rapidly with $\hat{k}_p$, decreasing correspondingly the time constant $1/\zeta_p\omega_p$. An increase in the frequency ω_p is desired so as to decrease the drift of the angular momentum vector caused by disturbances, and this is accomplished by incorporating the stiffness terms in the policy (17). With special values (27), the roots (33) simplify to

$$s = -\zeta_p\omega_p \pm j\omega_p\sqrt{1 - \zeta_p^2} \triangleq -\hat{k}_p/2 \pm j(1 + \hat{k}_p/2) \tag{38a}$$

$$\omega_p^2 = \hat{k}_p^2/2 + \hat{k}_p + 1, \qquad \zeta_p = \hat{k}_p/(2\omega_p) \tag{38b}$$

An interesting feature of the poles (38) is that ζ_p never reaches $1/\sqrt{2}$ regardless of $\hat{k}_p$, although the time constant is inversely proportional to $\hat{k}_p$.

Equations (34–38) provide convenient ways of choosing the precession gain $\hat{k}_p$. For instance, according to Eqs. (38), to reduce a 4-deg drift of angular momentum to, say, 0.004 deg (ignoring horizon sensor measurement errors) in one orbit, $\zeta_p\omega_p$ is set to be 1.1 and so $\hat{k}_p = 2.2$. Actual performance will be slightly different due to the variation in the magnetic field along the orbit, to the errors in measuring roll and estimating roll/yaw and their rates, and to the fact that the nutation damping gain k_n is not considered in arriving at the poles (34–38).

Nutation Damping

Because the nutation damping takes place over a short orbital arc (say, 10 deg), it is legitimate to ignore the precessional terms ($h_s\omega_0\alpha_1$ and $h_s\omega_0\alpha_3$) in Eqs. (13) and the precession gain k_p in the pitch dipole modulation law (6). Furthermore, it is now appropriate to consider the instantaneous roll/yaw components B_1 and B_3 of the magnetic field instead of using their orbit-average values, although the latter will be used subsequently to determine the orbit-average time constant for nutation damping. Moreover, ordinarily, the roll/yaw inertial angular rate components ω_1 and ω_3 of the spacecraft are related to the Euler angles and rates in the following manner:

$$\omega_1 = \dot{\alpha}_1 - \omega_0\alpha_3, \qquad \omega_3 = \dot{\alpha}_3 + \omega_0\alpha_1 \tag{39}$$

but when nutation damping is predominant, the inertial angular rates are essentially the Euler rates (that is, $\omega_1 \approx \dot{\alpha}_1$ and $\omega_3 \approx \dot{\alpha}_3$). In view of these comments, Eqs. (13), in the presence of nutation gain only, now modify to

$$I_1\dot{\omega}_1 + k_n B_3^2\omega_1 - (h_s + k_n B_1 B_3)\omega_3 = 0 \tag{40a}$$

$$I_3\dot{\omega}_3 + (h_s - k_n B_1 B_3)\omega_1 + k_n B_1^2\omega_3 = 0 \tag{40b}$$

By ignoring α_1 and α_3 and by writing Eqs. (40) in first-order form, the orbit mode, i.e., the mode associated with the momentum vector precession, is ignored and it is indirectly assumed that the precession part of α_1 and α_3 is constant during nutation. The characteristic polynomial associated with Eqs. (40) is

$$s^2 + sk_n\left(B_1^2 I_1 + B_3^2 I_3\right)/I_1 I_3 + \Omega_n^2 = 0 \tag{41}$$

where s is the Laplace variable associated with time t, not $\omega_0 t$ as before in Eq. (14). Let the uncontrolled ($k_n = 0$) root of Eq. (41) be denoted $s_0 \triangleq \pm j\Omega_n$ ($j^2 = -1$). Inasmuch as k_n effects nutation damping and does not influence the frequency Ω_n significantly, the complex root of the polynomial (41) will be $s = s_0 + \Delta s$ where the perturbation $|\Delta s| \ll \Omega_n$. Ignoring the second-order term $(\Delta s)^2$, it can be shown that

$$\Delta s = -s_0 k_n\left(B_1^2 I_1 + B_3^2 I_3\right)/\left[2s_0 I_1 I_3 + k_n\left(B_1^2 I_1 + B_3^2 I_3\right)\right] \tag{42}$$

To render Eq. (42) more useful, we recognize that the second term in its denominator is negligible compared to the first, because the gain k_n need be no greater than that required for the nutation damping coefficient ζ_n to be in the range 0.1–0.2. Therefore, the real part of Δs, denoted $-\zeta_n\Omega_n$, yields the time constant t_n equal to

$$t_n = 1/(\zeta_n\Omega_n) = 2I_1 I_3/\left[k_n\left(B_1^2 I_1 + B_3^2 I_3\right)\right] \tag{43}$$

which is a generalized form of Eq. (16) of Ref. 8 restricted to the inertially symmetric ($I_1 = I_3$) case. As the magnetic field components B_1 and B_3 vary with true anomaly [see Eq. (9)], the time constant t_n varies as well along the orbit, but it will never be negative or infinity, implying that ζ_n will never be zero or negative, the indicators of instability. At the ascending and descending nodes of the orbit relative to the geomagnetic equator (where $\omega_0 t - \eta_m = 0$ and π, respectively)

$$t_{n,\text{nodes}} = 2I_3/k_n' \tag{44a}$$

[see Eq. (12) for the definition of k_n']. Likewise, when the satellite is closest to the magnetic poles ($\omega_0 t - \eta_m = \pm\pi/2$), the time constant will be

$$t_{n,\text{poles}} = I_1/2k_n' \tag{44b}$$

To determine the orbit-averaged nutation damping, note that

$$\left(B_1^2\right)_{\text{av}} = \tfrac{1}{2}\hat{\mu}_m^2 \sin^2\xi_m, \qquad \left(B_3^2\right)_{\text{av}} = 2\hat{\mu}_m^2 \sin^2\xi_m \tag{45}$$

and, therefore, the average time constant $t_{n,\text{av}}$ and average nutation damping $\zeta_{n,\text{av}}$ are given by

$$t_{n,\text{av}} = 1/(\zeta_{n,\text{av}}\Omega_n) = 2I_1 I_3/\left[k_n'\left(\tfrac{1}{2}I_1 + 2I_3\right)\right] \tag{46}$$

Specifying $t_{n,\text{av}}$ or $\zeta_{n,\text{av}}$, the nutation gain k_n can be calculated easily from Eq. (46), knowing the remaining parameters. Also, the slight change in the nutation frequency, although not important, can be derived from Eq. (42).

V. Numerical Results and Discussion

Extensive numerical results were generated based on the preceding analysis, but due to space limitations only some of the results are shown here. Fuller results are presented in Ref. 15.

Precession and Nutation Damping Only (No Stiffening, $k_s = 0$)

The following results are obtained using the simplified linear Eqs. (13) and average roll/yaw control torques [Eqs. (18)] with $\hat{k}_s = 0$. Figures 1–4 compare root loci and damping coefficients associated with the orbit and nutation modes for a polar orbit satellite for two cases: a) when all states or their estimates are fed back and b) when all except yaw angle are fed back. The following parameters are used for illustration:

$$\begin{aligned} &h_s = -3 \text{ ft}\cdot\text{lb}\cdot\text{s}; \quad I_1 = 55.85, \quad I_2 = 34.98 \\ &I_3 = 37.67 \text{ slug}\cdot\text{ft}^2; \quad \omega_0 = 0.00104 \text{ rad/s}; \quad i = 108 \text{ deg} \end{aligned} \tag{47}$$

The time $t = 0$ is selected such that the magnetic field parameters $\xi_m = i + \gamma_m$ and $\eta_m = 0$ in Eqs. (9). The yaw and yaw rate feedback gains χ_p and χ_n in the policy (17) are set to be

$$\chi_p = I_1/I_3 = 1.48, \qquad \chi_n = I_3/I_1 = 0.675 \tag{48}$$

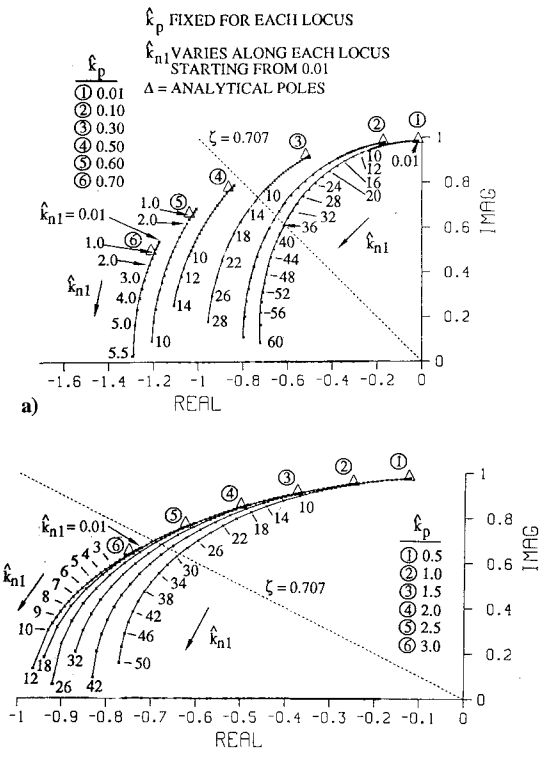

Fig. 1 Precession root loci for several fixed $\hat{k}_p$ and varying $\hat{k}_{n1}$ ($k_s = 0$): a) full-state feedback and b) no yaw feedback.

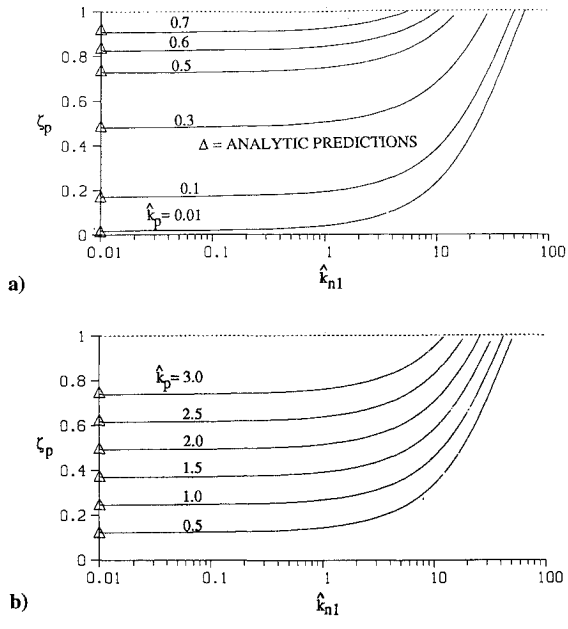

Fig. 2 Damping coefficient ζ_p associated with the precession poles in Fig. 1 ($k_s = 0$): a) full-state feedback and b) no yaw feedback.

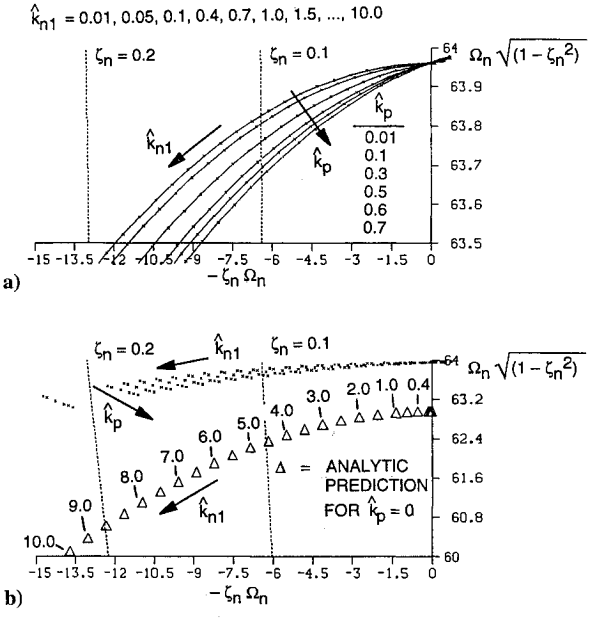

Fig. 3 Nutation root loci associated with full-state feedback and k_s = 0: a) numerical prediction and b) numerical and analytic predictions.

The parametric set (47) satisfies the approximation (1) because $|h_s|/I_1\omega_0 = 51.65$.

Figure 1a portrays the precession (orbit mode) root loci for $\hat{k}_p = 0.01, 0.1, 0.3, 0.5, 0.6$, and 0.7 when roll, yaw, and their rates are fed back. Each locus starts approximately from the pole Δ, Eq. (34), derived by ignoring the nutation mode. Figure 1a reveals that, in general, a precession gain $\hat{k}_p$ bestows significant damping to the orbit mode, enhanced further as the nutation gain $\hat{k}_{n1}$ increases. Figure 1b illustrates the orbit mode root loci without yaw feedback ($\chi_p = 0$ but $\chi_n = 0.675$) for $\hat{k}_p = 0.5, 1.0, 1.5, 2.0, 2.5$, and 3.0 (notice the larger $\hat{k}_p$ now). As in Fig. 1a, each locus in Fig. 1b starts from near the pole Δ [Eq. (37)]. Damping coefficients associated with the roots in Figs. 1a and 1b are illustrated in Figs. 2a and 2b. It is clear from Figs. 1 and 2 that in order to obtain the same level of damping and time constant in the precession mode, a substantially larger $\hat{k}_p$ is required if yaw is not fed back than if it is. We furthermore observe that the analytic predictions (Δ), Eqs. (35) and (37), of the damping coefficient ζ_p are quite accurate. The figures

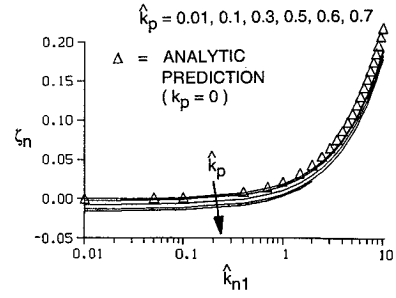

Fig. 4 Damping coefficients ζ_n associated with the nutation roots in Fig. 3; k_s = 0 and full-state feedback.

demonstrate that whereas the gain $\hat{k}_p$ (with $\hat{k}_{n1} = 0$) is eminently suitable for the momentum vector precession (or orbit mode damping) the gain $\hat{k}_{n1}$ (with $\hat{k}_p = 0$) can also be employed for this task, although that will require a large $\hat{k}_{n1}$ and roll/yaw rate estimates that may be noisy. The known destabilizing effect of the gain $\hat{k}_p$ on the high-frequency nutation mode is illustrated in Figs. 3 and 4 for full-state feedback. We observe in Fig. 3a that as $\hat{k}_p$ increases, the nutation roots associated with smaller $\hat{k}_{n1}s$ penetrate the right-half complex plane deeper and the corresponding damping coefficients (Fig. 4) become progressively more negative; therefore, for stability (that is, for damping) of the nutation mode, a larger $\hat{k}_{n1}$ gain is required. Figures 3b and 4 furthermore compare the nutation roots obtained numerically for nonzero $\hat{k}_p s$ with the analytic roots $s_0 + \Delta s$ [see Eq. (42)] with $k_p = 0$. The apparently large difference in the imaginary part of the roots in Fig. 3b is due to the magnified y scale. In Fig. 4, the analytic nutation damping coefficient ζ_n agrees very well with the numerical ζ_n for large $\hat{k}_{n1}$. Figure 4 also shows that as $\hat{k}_{n1}$ increases the precession gain $\hat{k}_p$ has progressively little influence on ζ_n, implying that if $\hat{k}_{n1}$ is selected for $\zeta_n \geq 0.1$, there is no fear of destabilizing influence of $\hat{k}_p$, and the nutation time constant will diminish just slightly (Fig. 3a). Figures 1–4 guide us to select the gains $\hat{k}_p$ and $\hat{k}_{n1}$ for desired stability and performance in both precession and nutation. For example, to reduce some initial roll/yaw error to its one-hundredth or one-thousandth value in one orbit period (2π rad), the real part in Fig. 1 must be -0.733 or -1.1, respectively. Figure 1a or 1b then furnishes a narrow range of $\hat{k}_p$ and $\hat{k}_{n1}$, depending on the control policy employed. Figures 3 and 4, on the other hand, dictate what $\hat{k}_{n1}$ must be for, say, $\zeta_n = 0.1$. Note that, because the nutation frequency is usually high relative to the orbit frequency (nearly 64 in Fig. 3), it is adequate to select ζ_n within 0.1–0.2, which then determines $\hat{k}_{n1}$. The foregoing selection of $\hat{k}_p$ and $\hat{k}_{n1}$ may be fine tuned subsequently using a detailed simulation.

The conclusions from Figs. 1–4 agree qualitatively with those of the prior investigators, but due to the averaging of the magnetic field, the reliability of the results must be established. The only exact way to do this is to examine the stability using Floquet theory. The space limitations forbid delving into these details here, but they are elucidated in Ref. 15 for the parameters

$$h_s = -4 \text{ ft} \cdot \text{lb} \cdot \text{s}; \qquad I_1 = 60.317, \quad I_2 = 56.12$$
$$I_3 = 44.443 \text{ slug} \cdot \text{ft}^2; \qquad \chi_p = 1.357, \quad \chi_n = 0.737 \tag{49}$$

and ω_0 and i as given by Eq. (47). Floquet analysis does not yield a literal stability inequality, and so the discrete pairs of $\hat{k}_{n1}$ and $\hat{k}_p$ at the stability boundary circle of unit radius are symbolized in Fig. 5 and compared with the Routh–Hurwitz stability boundaries $\Delta_3 = 0$ [Eq. (15)] for both full-state feedback and no yaw feedback, using the parameters of Eqs. (49) (with $k_s = 0$). Quite surprisingly, Floquet stability demarcations agree remarkably well with the linear, average stability boundary in Fig. 5. This figure illustrates additional stability boundaries (25), (26a), and (26b) denoted 1, 3, and 2, respectively, in Fig. 5. The conditions (26) are derived under the assumption that $\chi_n = 1$ (yaw rate feedback) and $\chi_p \approx 0$ (almost no yaw feedback). Despite a slight difference in the χ_n, the boundary (26a) (or 3) for $\chi_n = 1$ agrees with the Floquet and Routh–Hurwitz stability results for $\chi_n = 0.737$. The conditions (25) (or 1) and (26b) (or 2), however, disagree marginally with the other boundaries

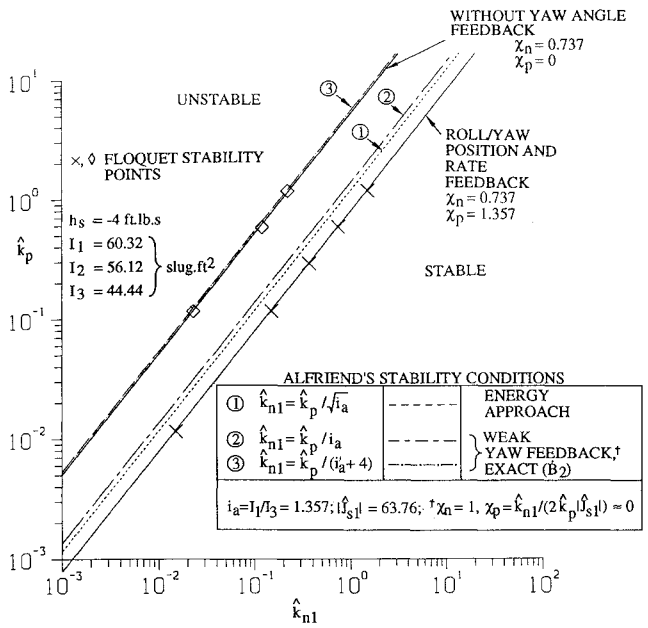

Fig. 5 Stability regions for controllers with and without yaw feedback; comparison with the stability boundaries from Refs. 6 and 8; labels stable and unstable were inadvertently exchanged in Fig. 7 of Ref. 15.

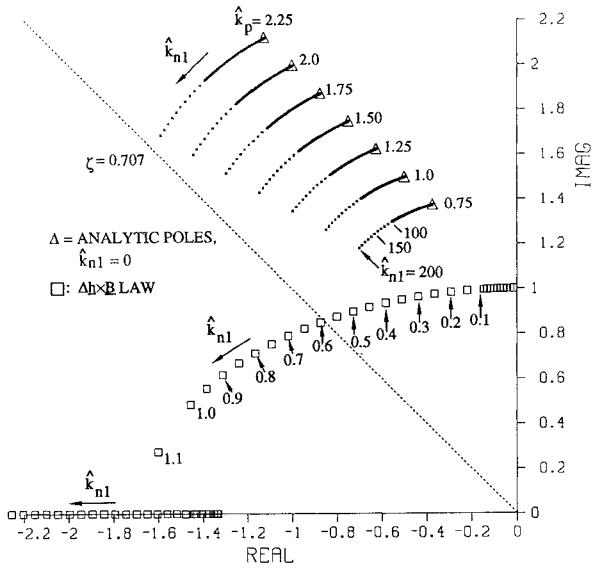

Fig. 6 Precession root loci for the controller with stiffness gain and $\Delta h \times B$ controller.

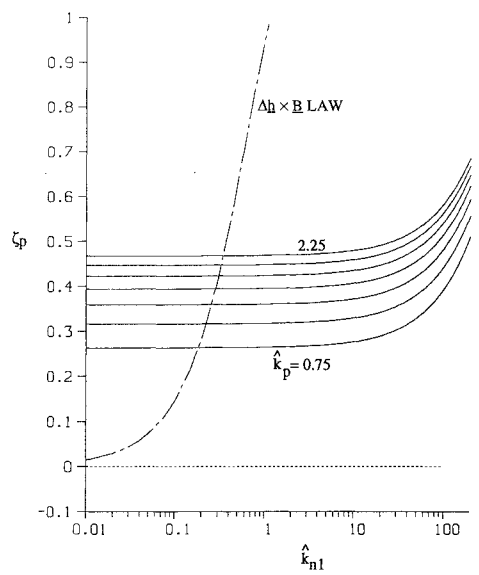

Fig. 7 Damping coefficients of the orbit mode roots in Fig. 6.

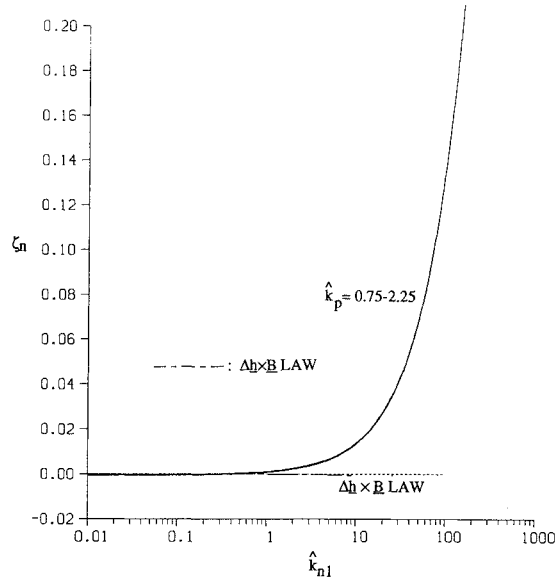

Fig. 8 Nutation damping coefficients associated with the precession roots in Fig. 6.

because of the differences in the χ_n and χ_p, as we shall see further in Fig. 8.

Controller with Precession, Nutation Damping, and Stiffness, and $\Delta h \times B$ Policy

Figures 6 and 7 portray the closed-loop root loci and damping coefficients associated with the policy (17) with special values [Eq. (27)] of parameters. These results are obtained by eigenanalysis of the simplified equations of motion (13) along with the average control torques (28) and (29). They are compared with the results of the $\Delta h \times B$ controller for which the stiffness gain k_s is zero, the nutation and precession gains are related according to Eq. (25) (which is actually the stability boundary), and χ_p and χ_n are both unity. The numerical results in this section pertain to the moments of inertia in Eq. (49), but h_s and ω_0 are now $h_s = -60$ ft · lb · s, $\omega_0 = 0.6886$E-3 rad/s. Comparing the orbit mode root loci in Fig. 6 with those in Figs. 1a and 1b (for which $k_s = 0$), the advantage of the stiffness gain $k_s[\hat{k}_s = \hat{k}_p/4$, the nondimensional version of the relationship (27a)] is apparent: larger negative real parts, implying smaller time constants and faster convergence to the origin, and larger imaginary parts, implying smaller steady-state oscillations or better pointing accuracy under environmental disturbances. The symbol Δ in Fig. 6 at the beginning of each root locus is the analytic root (38) derived for zero nutation gain. Since the first value, 0.01, of the nutation gain $\hat{k}_{n1}$ is essentially zero, the analytical and numerical roots agree closely. Regarding $\Delta h \times B$ law, Figs. 6 and 7 show that large negative real parts and damping coefficients corresponding to the orbit mode can be obtained using this law, but Fig. 8 demonstrates that it is completely unable to provide nutation damping, whereas, in contrast, for the policy (17), an appropriate gain $\hat{k}_{n1}$ can be selected easily for nutation damping coefficient equal to 0.1–0.2.

These stability results, based on the average magnetic field, concur with Floquet stability results. Five stability boundary pairs of $\hat{k}_p$ and $\hat{k}_{n1}$ from Floquet theory for the Lebsock–Eterno law are laid out in Fig. 9 (identified by the symbol ◊). In addition, this figure displays the linear, average, stability boundary $\Delta_3 = 0$ for 1) Lebsock–Eterno law, 2) roll/yaw position and rate feedback with $k_s = 0$ and $\chi_n = 1 = \chi_p$, and 3) the relationship (25), denoted boundary 1 earlier in Fig. 5, between precession and nutation gains according to $\Delta h \times B$ law. First we observe that, for the Lebsock–Eterno law, the pairs of parameters for Floquet stability agree very well with the linear, average stability boundary. The threshold $\hat{k}_{n1}$ for the Lebsock–Eterno law for a specified $\hat{k}_p$ is much less than that

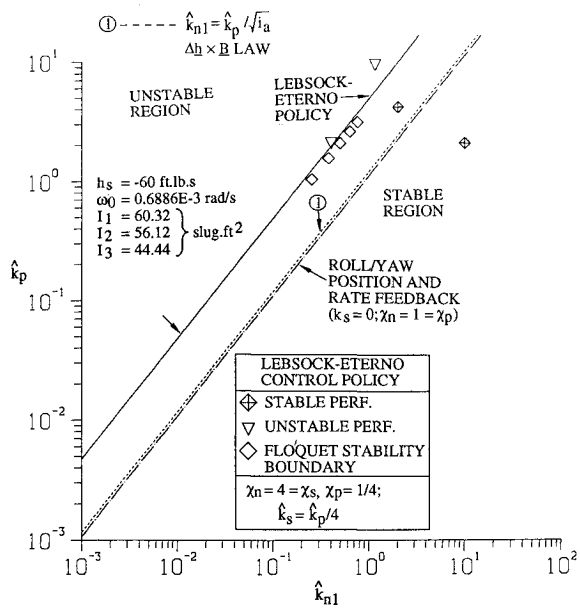

Fig. 9 Stability boundaries predicted by Lebsock–Eterno law ($k_s \neq 0$), and roll/yaw position and rate feedback with $k_s = 0$, $\chi_n = 1 = \chi_p$; comparison with $\Delta h \times B$ policy and Floquet stability predictions.

for case 2 because a stiffness gain augments the system stability. On the other hand, the stability boundaries corresponding to the cases 2 and 3 are, as eagerly hoped for, essentially the same. Note that the stability boundary in Fig. 5 pertaining to the roll/yaw angle and rate feedback, similar to the case 2, is for $\chi_n = 0.737$ and $\chi_p = 1.357$. Finally, Fig. 9 includes two examples of stability (Φ) and one example of instability (∇) as inferred from the time-domain simulation of the more complete equations of motion, Eqs. (6.4.25) of Ref. 12, with the control torque based on the varying magnetic field and Lebsock–Eterno policy and the initial condition $\alpha_1 = -4$ deg. It is confirmed from Fig. 9 that the time-domain stability results are in harmony with the Routh–Hurwitz or Floquet stability results. Actual precession and nutation damping plots in the time domain are shown in Ref. 15.

VI. Concluding Remarks

The classical $\Delta \boldsymbol{h} \times \boldsymbol{B}$ magnetic attitude controller—eminently suitable for momentum removal or, equivalently, precession of momentum-bias satellites—does not provide nutation damping at all because it precludes independent selection of precession and nutation gains, both being linked by a relationship. The two-gain magnetic controllers are required therefore, in order to perform both precession and nutation damping. Stability and performance characteristics of these laws, however, depend significantly on whether both roll and yaw or roll alone are fed back to determine the instantaneous pitch dipole strength. Feeding back both roll and yaw (or their estimates) is advantageous because then the direction of the drifted angular momentum vector in the celestial sphere is known completely and the time constant to bring the momentum vector to its intended orientation will be considerably shorter than when only roll is fed back. For still superior performance, especially for tighter pointing accuracy under persistent external disturbances, three-gain laws that include the terms that stiffen the roll/yaw motion directly are desired because the enhanced frequency diminishes the momentum vector drift. For more cohesion in the literature, all of these magnetic attitude controllers are analyzed, compared, and tied with the laws and the results of the past. Precession roots and nutation damping coefficients are related with the gains, facilitating their determination for specified pole locations. Finally, Routh–Hurwitz stability boundaries between precession, nutation, and stiffness gains, using averaged magnetic field, agree remarkably well with the discrete stability points arrived at using Floquet theory.

References

[1]Lindorfer, W., and Muhlfelder, L., "Attitude and Spin Control for TIROS Wheel," *Proceedings of the AIAA/JACC Guidance and Control Conference* (Seattle, WA), AIAA, New York, 1966, pp. 448–462.

[2]Hawkins, P. J., and Clark, J. P. C., "Autonomous Magnetic Attitude Control System of the AEM Base Module," *Proceedings of the AIAA Guidance and Control Conference* (Boulder, CO), AIAA, New York, 1979, pp. 476–483.

[3]Lebsock, K., and Eterno, J., "Design of a Maneuverable Momentum Bias Attitude Control System," *Proceedings of the AIAA/AAS Astrodynamics Conference* (Minneapolis, MN), AIAA, Washington, DC, 1988, pp. 704–713.

[4]Wheeler, P. C., "Spinning Satellite Attitude Control via the Earth's Magnetic Field," *Proceedings of the AIAA/JACC Guidance and Control Conference* (Seattle, WA), AIAA, New York, 1966, pp. 97–108.

[5]Wheeler, P. C., "Spinning Spacecraft Attitude Control via the Environmental Magnetic Field," *Journal of Spacecraft and Rockets*, Vol. 4, No. 12, 1967, pp. 1631–1637.

[6]Alfriend, K. T., "Magnetic Attitude Control System for Dual-Spin Satellites," *AIAA Journal*, Vol. 13, No. 6, 1975, pp. 817–822.

[7]Sorensen, J. A., "A Magnetic Attitude Control System for an Axisymmetric Spinning Spacecraft," *Journal of Spacecraft and Rockets*, Vol. 8, No. 5, 1971, pp. 441–448.

[8]Stickler, A. C., and Alfriend, K. T., "Elementary Magnetic Attitude Control System," *Journal of Spacecraft and Rockets*, Vol. 13, No. 5, 1976, pp. 282–287.

[9]Goel, P. S., and Rajaram, S., "Magnetic Attitude Control of a Momentum-Biased Satellite in Near-Equatorial Orbits," *Journal of Guidance and Control*, Vol. 2, No. 4, 1979, pp. 334–338.

[10]McElvain, R. J., "Satellite Angular Momentum Removal Utilizing the Earth's Magnetic Field," *Torques and Attitude Sensing in Earth Satellites*, edited by S. F. Singer, Academic, New York, 1964, pp. 137–158.

[11]Plett, M., "Magnetic Field Models," *Spacecraft Attitude Determination and Control*, edited by J. R. Wertz, D. Reidel, Dordrecht, The Netherlands, 1978, pp. 779–786.

[12]Hughes, P. C., *Spacecraft Attitude Dynamics*, Wiley, New York, 1986, Sec. 11.3, pp. 455–460.

[13]Ergin, E. I., and Wheeler, P. C., "Magnetic Attitude Control of a Spinning Satellite," *Journal of Spacecraft and Rockets*, Vol. 2, No. 6, 1965, pp. 846–850.

[14]Lebsock, K. L., "Magnetic Desaturation of a Momentum Bias System," *Journal of Guidance, Control, and Dynamics*, Vol. 6, No. 6, 1983, pp. 477–483.

[15]Hablani, H. B., "Comparative Stability Analyses and Performance of Magnetic Controllers for Momentum Bias Satellites," *Proceedings of AAS/GSFC International Symposium on Space Flight Dynamics* (Greenbelt, MD), NASA Goddard Space Flight Center, 1993, pp. 1–18 (Paper 93-278).